Imaging measurement technologies for CCS

Yessica Arellano[1*], Stian Husevik Stavland [2], Elvia Chavez Panduro [1], Børge Hamre [2], and Bjørn Tore Hjertaker [2]

[1] *Department of Gas Technology, SINTEF Energy Research, Trondheim, Norway*
[2] *Department of Physics and Technology, University of Bergen, Bergen, Norway*
** e-mail: yessica.arellano@sintef.no*

***Abstract*— Carbon Capture and Storage (CCS) is seen as a key strategy on the path to net-zero emission. Measurements of carbon dioxide-rich mixtures are vital for the forthcoming widespread implementation of CCS. The present study investigates the opportunities for use of tomography throughout the CCS value chain. Tomographic methods offer significant promise in measuring a broad spectrum of properties. Such measurements rely on the identification of contrasting properties from different substances. For tomographic technology to be a viable solution, the timescale and spatial resolution must be sufficient to capture the dynamics of the process being monitored. The present work evaluates to what extent foreseen changes in the properties of various CCS processes can be detected by tomographic measurements. The findings of the study disclose that tomography systems may offer advantages in monitoring and measuring CCS processes. Multimodal configurations could broaden the applicability of tomographic methods, especially in combination with fiscal meters or in scenarios where water presence is foreseen, like post-capture processes involving amines. However, further studies and experimental verification is required prior to widespread use.**

Keywords*— Flow measurement, tomography, carbon dioxide, CCS, capture, transport, storage, dry ice, leak detection

I. INTRODUCTION

Carbon capture and storage (CCS) is key to mitigate the climate changes caused by emissions of greenhouse gases [1, 2]. Early strategies for CCS focused on capturing CO_2 from fossil fuel power plants and point-to-point transport. More recently, there has been increased attention on CO_2 capture from various industrial sources [3] with the natural derivation of CCS developments arranged in clusters.

CCS comprises three main processes, (i) capture and conditioning of CO_2 from emitting sources, followed by (ii) transportation of the CO_2 to a storage site, where it is (iii) permanently stored in underground geological formations. Different CO_2 emitters (cement, steel, petrochemicals, biofuel, etc) require dedicated capture solutions, depending on the conditions such as available concentration of CO_2, pressure, available heat, transport solution, and whether the capture process will have to be a retrofit or can be integrated into a new process plant. Correspondingly, the diversity of capture processes and of the CO_2 sources lead to an assortment of impurities and compositions. Transport and storage requirements dictate the maximum concentrations of non-condensable, hazardous, and corrosive species in the CO_2 streams. Typical impurity limits of existing projects are listed in TABLE I.

TABLE I. SPECIFICATIONS OF IMPURITY CONTENT (ADAPTED FROM [4])

	H_2O	**H_2S**	**CO**	**SOx**	**NOx**
v/v [ppm]	30-500	9-100	35-900	10-25000	10-2000

Solutions are needed along the value chain for flow measurements, process control, flow assurance, inventory tracking, and leak detection, among others [5]. Streams of CO_2 from different industrial sources yield large local and temporal variations in flow rates and operating conditions with various flow assurance issues. Further, CCS transport takes place close to the vapour-liquid equilibrium curve of CO_2, where properties change rapidly with temperature and pressure [6, 7]. The challenges above call for flow measurement solutions, where tomography could be valuable. For CCS storage, well and reservoir integrity, leak detection, and storage capacity are topics where tomographic measurement could give valuable insight.

Tomography is a technique to obtain 2D or 3D image representation using different types of penetrating waves. There have been few tomography applications for CCS, as per the limited bibliography available. Among the most relevant are investigations of electrical tomography for use in CCS-like streams. Cross-sectional distribution of two-phase CO_2 was successfully monitored by capacitance tomography (ECT) at reportedly 6% accuracy [8]. ECT and ultrasound tomography have been the subject of lab studies to monitor CO_2 capture processes with $CaCO_3$ precipitation within the Tomocon project [9, 10]. On a larger scale, pilot tests for geological monitoring of CO_2 via resistive tomography (ERT) were successfully undertaken in the Northeast German Basin [11].

The present work intends to build on the explored potentialities thus far and provide an overview of the prospective niches for various tomography techniques along the CCS value chain. Potential uses of tomographic measurement technology for CCS comprise (1) field deployment, leveraging specific technology-based knowledge as per experiences in industrial processing monitoring and measurement as redundancy measurements or to complement other measurement methods; (2) laboratory-based research to shed light on the flow behaviour of CO_2 and the physicochemical interaction with various common reservoir compounds; and (3) development, characterisation and customisation of measuring instruments where the exploitation of tomographic and tomometric (time series of raw measurement without image reconstruction) methods can improve the measurement confidence by using their capabilities to accurately map the distribution of the phases and components in the pipe cross-section based on intrinsic properties of the fluids [12-15].

This is the accepted version of an article published at the 2022 IEEE 12th Sensor Array and Multichannel Signal Processing Workshop (SAM)
https://doi.org/10.1109/SAM53842.2022.9827823

II. Tomography Sensing Principles

There exist various tomography modalities, the choice of which largely depends on the fluid type and the operating conditions. TABLE II is a non-exhaustive list of promising techniques for CCS. A third class of tomography techniques, based on acoustic imaging, may also be promising for CCS; yet, the inherently different interrogation and acquisition basis of such techniques is past the scope of this work.

In radiative tomography, the attenuation of electromagnetic waves is reliant on the scattering and absorption properties of the material. Depending on the photon energy of the radiation, different physical processes determine and dominate the scattering and absorption. Broadly, the methods can be separated into two categories: diffuse tomography (DT), which relies on a scattering dominant transfer regime, and single scatter -and absorption- tomography (SST), when the radiative transfer is mostly dependent on absorption and single scatter. While DT methods generally contain more information, and can be used to image more accurately, it is also more complex and requires advanced models and reconstruction algorithms. In SST, instead, measurements can be approximated by the Beer-Lambert exponential decay law, and traditional linear solvers can be used for reconstruction.

Gamma-ray (GRT) and X-ray (XRT) tomography use radiation photon energy in the range from 100eV to 1 MeV. The optimal choice of radiation type depends on the measurement geometry and materials, including piping and fluid components. The photon energy range is dominated by photoelectric absorption (PE) at the lower end and Compton scattering at the high end, for which the linear attenuation is approximately proportional to the density of matter. A typical GRT configuration consists of five radioactive sources with corresponding detectors arranged in a circular geometry [16, 17]. The spatial resolution mainly depends on the number of detectors but also on the source size and the scattering properties. For XRT, the most common configuration is an X-ray source and a single large array or matrix detector. The tomography measurements are performed by rotating the sample or the detector. Both GRT and XRT can, in principle, measure through steel walls, especially at high energy levels. Yet, workarounds may be needed to reduce attenuation in casing and pipe walls. The temporal resolution of GRT and XRT is contingent both on the contrast between components and the source intensity. In advanced laboratory setups, the resolution increases significantly.

Optical tomography (OT) modalities include both optical DT (ODT) and optical SST [18, 19]. In addition to measurements in the visual spectrum, infra-red (IR) and ultra-violet are also included in what is considered optical measurements. ODT can be based on scattered light, fluorescence, or bioluminescence. SST methods are used when absorption or single scatter is dominant, and multiple scatters are negligible. Multispectral measurements may be used for solving multi-component problems where different spectral dependencies between the components exist. OT demands optical access, which typically means pressure-resistant lenses. OT would also be sensitive to deposits on the lenses and may require cleaning.

TABLE II. Principles of operation for process tomography

	Modality	Sensitivity	Comments
Radiation	Optical	Optical absorption & scatter, [a]Density	Optical access required
	X-ray and γ-ray	Mass attenuation coefficient, Density	Radiation confinement X-ray limited to laboratory
	Magnetic resonance	Relaxation time, [a]Density	Expensive for large vessels
Electric	Capacitive	Dielectric permittivity	Scalable to small or large diameters. On-line, non-radioactive. High TRL, low cost Non-conductive fluid enclosure required.
	Conductivity	Conductivity	
	Inductive	Conductivity, [a]Permittivity	
	Impedance	Conductivity	

[a]Secondary sensitivity

For magnetic resonance imaging (MRI), the main core of the acquisition process is based on the phenomenon of Nuclear Magnetic Resonance (NMR). According to Elkins et al. [20], the intensity measured is based on parameters such as (i) the type of nucleus under study, like ^{1}H, ^{13}C and others. ^{1}H protons are the most common – in this case, molecules containing H atoms like H_2O will be visible but not, e.g. CO_2 or N_2 – (ii) the density of the sample, and (iii) the relaxation time. Velocities can also be measured using MRI without needing an additional measurement plane as in [21], and unlike other techniques, this is the only method where different velocities generate contrast.

In non-radiative electromagnetic tomography, the differences between the electromagnetic properties of the components give rise to variations in the inter-sensor measurement. Different techniques rely on capacitive, conductive, impedance, or induction measurements. Thorough descriptions of their operating principle are broadly available in the literature, e.g., in [22]. Given a set of measurements, the distribution of the electromagnetic properties across the imaging region can be approximated. The relationship between the measured signals and the variations in the electromagnetic property of interest is often non-linear [23]. Hence in practice, it is necessary to use empirical means based on experiments to determine the appropriate correction factor to use when calculating the mixture concentration from the measured property. Further, electromagnetic tomography requires electrical coupling to the process via, for example, a non-conducting spool piece.

The sensitivity of the sensors to changes in the electromagnetic properties varies with the concentration of the species and their distribution within the imaging region. Achieving a high spatial resolution requires a reasonable estimation of the measured signals with low uncertainty, which must represent the physical phenomena. Temporal resolution is typically high, up to 0.1 ms.

This is the accepted version of an article published at the 2022 IEEE 12th Sensor Array and Multichannel Signal Processing Workshop (SAM)
https://doi.org/10.1109/SAM53842.2022.9827823

III. Benchmarking

This section assesses the potentialities and limitations of using tomographic methods in CCS.

A. CO_2 Capture and Transport

In TABLE III, compositions are provided of CO_2-rich streams for various capture processes averaged from the ranges provided in [24] and for that of transport conditions considered in the Northern Lights project [6]. Fluid properties were estimated using the models recommended in the NIST REFPROP v9.0 tool [25]. Dielectric constant computation is documented in [26].

X- and γ-ray radiation are stochastic processes where a certain number of counts is necessary to achieve sufficient accuracy, e.g., 10000 counts yield an uncertainty of 1 %. The count rate is, in addition to source intensity, dependent on the mass attenuation coefficient of composition, density, and length through the material. Care must be taken to optimise these with respect to the application. For industrial CO_2 transport, the pipe diameter would typically range from 20 to 30 cm. Fig. 1 shows the normalised intensity at photon energy levels from 1 keV to 10 MeV for different CCS streams (see TABLE III) with a pathlength of 25 cm. The photon energy should be chosen so that the count rate at normal conditions is sufficiently high. The lower cut off varies with the density and is approximately 5keV for the post-combustion scenario, 20 keV for pre-combustion, and between 50 and 90 KeV for the remaining.

Another limiting factor is the contrast among different components. Detection using γ- or X-ray of small impurities dissolved in gas or liquid could prove unfeasible as this is dependent on the components having significantly different mass attenuation coefficient. But our estimation indicates that there are some contrasts for argon and H_2S, and for the lighter elements H_2 and CH_4, in the energy range where the photoelectric effect is significant. Also, for a component condensed from the gas stream or evaporated from liquid, it is possible to measure if there is a significant density difference, see TABLE III.

In the IR region, the radiative transfer of electromagnetic waves is dominated by absorption and can therefore be approximated by the Beer-Lambert law. Fig. 2 shows absorption lines for some gases estimated using the HITRAN database [27]. The absorption lines are calculated at 240 K and 1MPa utilising a composition of 96 % CO_2 and 1 % of each of the other gases. As can be seen, several wavelengths give a good contrast between H_2O and CO_2. But also, other components can potentially be resolved. Arrows indicate isolated peaks where all components can be easily identified, except for CH_4 and CO which are co-located. This suggests that by using multispectral measurements, more components can be quantified. Solids, or liquid in gas, or gas in liquid would result in scattering. It is assumed that small fractions of this could be detected, either by SST or DT techniques.

The contrasting electromagnetic properties of the components of the CO_2-rich streams can also be leveraged by non-radiative tomography techniques. The sensitivity of the electric-based modes of TABLE II suggests that only capacitance and magnetic induction tomography (ECT and MIT, respectively) could, in principle, detect variations in CCS streams since CO_2 is not conductive. The dielectric constant of common species at a component level and at process conditions is listed in TABLE III. The contrast between the CO_2 and common impurities, other than water, for pipeline, shipping and oxyfuel capture can be potentially detected by ECT, as found feasible elsewhere [28-30], provided water fractions are low to avoid parasitic coupling [31].

On the other hand, measurement of the permittivity ranges expected could be impractical to measure via MIT. Although in [32] it was proven that inductive tomography is sensitive to dielectric variations in the order of 1.06, the reported contrast corresponded to 100% of volumetric changes. Moreover, such permittivity change yielded small

TABLE III. Properties of common components in CCS stream

	Oxyfuel	**Pre-Combustion**	**Post-Combustion**	**Pipeline**	**Shipping**
Pres [MPa]	11	5.1	0.2	11	1.5
Temp [K]	308	312	313	278	243
Density ρ [kg/m^3]					
CO_2	744	117	3.41	955	1076
O_2	143	64	2.46	165	24
N_2	119	55	2.15	134	21
Ar	179	80	3.07	205	30
H_2O	999	995	992	1005	-
H_2	8	4	0.16	9	1.5
CH_4	80	34	1.24	97	13
Mixture	633	126	3.7	955	1076
Dielectric constant [–]					
CO_2	1.456	1.061	1.002	1.595	1.685
O_2	1.054	1.024	1.001	1.062	1.009
N_2	1.057	1.026	1.001	1.065	1.010
Ar	1.057	1.025	1.001	1.065	1.010
H_2O	75.29	73.72	73.20	86.36	-
H_2	1.025	1.012	1.001	1.027	1.005
CH_4	1.101	1.042	1.002	1.124	1.016
Mixture	1.414	1.062	1.028	1.597	1.684

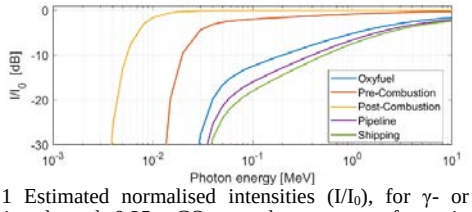

Fig. 1 Estimated normalised intensities (I/I_0), for γ- or X-ray radiation through 0.25m CO_2, vs. photon energy for typical CCS densities.

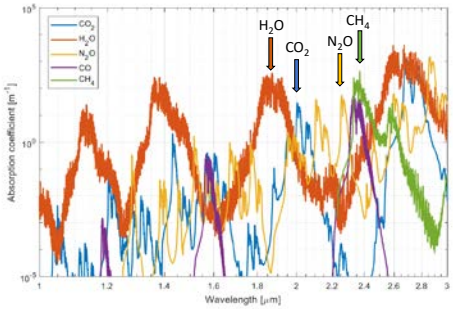

Fig. 2 Absorption coefficients for CO_2, H_2O, N_2O, CO, and CH_4 as functions of wavelength in the infrared region at 1 µm - 3 µm and 1 MPa.

This is the accepted version of an article published at the 2022 IEEE 12th Sensor Array and Multichannel Signal Processing Workshop (SAM)
https://doi.org/10.1109/SAM53842.2022.9827823

shifts in the measured voltage (in the milliVolts range). Hence, given the current readiness level of the technology, MIT measurements of non-conductive minor species in the CO_2-rich stream seems unfeasible.

Besides the above potential of the technologies to function independently, multimodal measurement can prove beneficial [21]. For example, a dual setup could consist of one technology sensible to fluid conductivity, like MIT or ERT and an adjacent system able to differentiate CO_2 and water from impurities, e.g., GRT or ECT. Regarding the latter, calibrating the ECT to low permittivity constants like suggested in [31] allows to combine CO_2 and traces of H_2O to appear similar in the reconstructed tomogram. The method is also valid for tomometric and average measurements across a homogeneous distribution.

Coupling tomographic measurements to non-tomographic measurement technologies offer opportunities for enhancing measurement accuracy and assisting real-time measurement corrections based on, for example, reconstructed phase distributions. Further, tomographic and tomometric techniques can be exploited to ensure accuracy of adjacent metering devices. The variety of compositions of CO_2-rich streams can significantly affect flow meters' performance. This is especially relevant for flow meters that are composition-sensitive or, that operate close to critical or, as is the case of fiscal metering in ship offloading, close to saturation conditions. The colocation of a tomography device in the proximity of a meter can be advantageous to identify phase transitions, which compromise the metering accuracy of most fiscal metering technologies [33].

B. CO_2 Storage

Permanent storage of CO_2 calls for investigation of reservoir and caprock integrity, reservoir capacity, injectivity, and leak detection. The contrasting properties of the relevant components can be leveraged by XRT, MRI, and ERT to monitor reservoir conditions. XRT and GRT have been used to monitor samples exposed to CO_2 under reservoirs conditions [34], given the difference in density between the rock material and CO_2 (see TABLE IV). The low conductivity of CO_2, up to three times lower than brine, has been utilised for CO_2 plume detection in ERT pilots [35]. Such experience suggests that MIT could also be used for leak detection, subsurface and reservoir characterisation, and plume tracking. MRI tomography is also a promising technique for core flooding experiments, as presented in [36]. Similarly, in theory, differences in the electromagnetic properties between water and other components could also be utilised by electric-based techniques through sensor integration within core flooding systems.

IV. Special Flow Assurance Cases

Besides the above potentialities and limitations of tomography for operational monitoring of CCS, their use for flow assurance is discussed in the following.

A. Dry ice detection

Ship transport of CO_2 normally takes place in 10000m^3-capacity ships and is presently routinely performed at operational conditions of around 1.5 MPa and 247 K. However, the economic feasibility of larger-scale ships mandates lower pressure transport (0.6-0.7 MPa) [37]. A crucial safety and operational aspect, particularly at low transport pressures, is the possible dry-ice formation while venting CO_2 [4], during liquefaction [38], or due to other transient pressure drops. Dry ice can result in the clogging of tubes, valves, and other narrow channels. The formation of solid CO_2 surrounded by liquid or gaseous CO_2 could be detected by OT by SST for early dry ice detection or DT. OT images of the liquid surface can also give information on the presence of floating dry ice, i.e. in case there are gas bubble on it. Still, optical access is required. GRT is also feasible, given the density contrasts between liquid (~1100 kg/m^3) and solid CO_2 (~1600 kg/m^3). ECT can also be an alternative, so long the permittivity contrast allows it. Note that dry ice permittivity which ranges between 1.4 and 2.1 [39], can be quite similar to that of liquid CO_2 at shipping conditions (~1.7 – see TABLE III).

TABLE IV. Density and permittivity of common reservoir components at storage conditions (15MPa and 350K)

Storage components	ρ [kg/m^3]	Dielectric constant [–]
CO_2 [25]	450	1.3
Water [25]	980	62
Sandstone [40]	~2600	16
Shale [40]	1970-2020	20-49
Cement [34]	~2005	13

B. Pipeline leakage and integrity monitoring

Monitoring transport operations is valuable to extend pipeline integrity and detect leaks. Leak detection through continuous pressure and temperature monitoring and regular sampling is customary. It is impractical for long pipeline systems to rely on flow measurement layouts at short and regular intervals, while pipeline inspection can prove expensive and disruptive. Tomographic methods accompanying pressure and temperature monitoring could circumvent some of these operational challenges. Tomography can sense major shifts in the composition and identify phase changes, which could yield water deposition in low points that cause corrosion. Field-deployable setups of the spool type or clamp-on arrays that can be installed on any existing pipeline or moved to desired locations are commercially available or close to market-ready from several providers [41-44].

V. Conclusions

Successful tomography implementation within the CCS value chain may offer improved process control and flow assurance monitoring. Tomography can also be used in R&D laboratories for a better understanding of the CCS processes, especially for CO_2 storage, and as reference measurement for the development of other technologies. There are no general tomographic solutions for CCS. Rather, there are different modalities whose sensitivity can be leveraged in specific processes therein. The density-based techniques, i.e., GRT, XRT and, to some degree, electromagnetic tomography, are mostly sensitive to components that are separated into different phases, e.g., evaporated gas from liquid, dry ice in a liquid stream, etc. On the other hand,

This is the accepted version of an article published at the 2022 IEEE 12th Sensor Array and Multichannel Signal Processing Workshop (SAM)
https://doi.org/10.1109/SAM53842.2022.9827823

optical methods can measure small quantities of dissolved components in CO_2, as well as the early onset and small fractions of condensation, evaporation, or solid formation. Further, tomographic imaging is only one aspect of the available information. Tomometric and bulk measurements of streams are, with inherent redundancy, also readily available and broadly applicable. Nonetheless, measurement access to the process, key for implementation of tomography, can be challenging, especially at high pressures.

This study mainly addressed specific post-capture applications, primarily focusing on transport and storage. However, tomography could provide even better prospects within conditioning and capturing processes where a wider repertoire and larger concentrations of components other than CO_2 are present. The application of the various benchmarked tomographic methods requires more work, as none have been extensively tested for CCS applications. Technological readiness level and equipment costs also require further assessment, as variations among the proposed methods can influence their applicability.

ACKNOWLEDGMENT

This publication has been partially funded by The Norwegian Research Council and produced under the project N° 327056 Monitoring and Control of CCS networks – MACON CCS. The authors acknowledge the following partners for their contributions: KROHNE, NeO, NTNU, ROXAR, and TECHNIP FMC.

REFERENCES

[1] "Energy Technology Perspectives 2017," International Energy Agency, Paris, France, http://www.iea.org/etp/, 2017.
[2] V. Masson-Delmotte et al., Eds. Global Warming of 1.5°C. https://www.ipcc.ch/sr15/ IPCC, 2018
[3] "World Energy Outlook," IEA, 2020. [Online] www.bit.ly/WEO_
[4] A. Moe et al., "A Trans-European CO2 Transportation Infrastructure for CCUS: Opportunities & Challenges," ETIP ZEP, https://zeroemissionsplatform.eu/ 2020.
[5] C. Mills, "Flow Measurement in support of Carbon Capture, utilisation and Storage (CCUS)," TUV SUD NEL, 2021, vol. 2021_299. [Online]. https://www.instmc.org/
[6] Northern Lights. "Accelerating decarbonisation." https://northernlightsccs.com/
[7] H. Hollander, E. Jukes, S. W. Løvseth, and Y. Arellano, "The challenges of designing a custody transfer metering system for CO_2" in North Seas Flow Measurement Workshop, 2021, vol. 39.
[8] S. Sun, W. Zhang, Z. Cao, L. Xu, and Y. Yan, "Real-time imaging and holdup measurement of carbon dioxide under CCS conditions using electrical capacitance tomography," IEEE Sensors Journal, vol. 18, no. 18, pp. 7551-7559, 2018.
[9] P. Koulountzios, S. Aghajanian, T. Rymarczyk, T. Koiranen, and M. Soleimani, "An Ultrasound Tomography Method for Monitoring CO2 Capture Process Involving Stirring and CaCO3 Precipitation," Sensors, vol. 21, no. 21, p. 6995, 2021. [Online] https://www.mdpi.com/1424-8220/21/21/6995.
[10] S. Aghajanian, G. Rao, V. Ruuskanen, R. Wajman, L. Jackowska-Strumillo, and T. Koiranen, "Real-Time Fault Detection and Diagnosis of CaCO3 Reactive Crystallization Process by Electrical Resistance Tomography Measurements," Sensors, vol. 21, no. 21, p. 6958, 2021. [Online] https://www.mdpi.com/1424-8220/21/21/6958.
[11] C. Schmidt-Hattenberger et al., "Monitoring of geological CO_2 storage with electrical resistivity tomography (ERT): Results from a field experiment near Ketzin/Germany," in International Workshop on Geoelectric Monitoring, 2011: Citeseer, p. 75.
[12] S. H. Stavland, C. Sætre, B. T. Hjertaker, S.-A. Tjugum, A. Hallanger, and R. Maad, "Gas fraction measurements using single and dual beam gamma-densitometry for two phase gas-liquid pipe flow," in 2019 IEEE International Instrumentation and Measurement Technology Conference (I2MTC), 2019: IEEE, pp. 1-6.
[13] E. M. Bruvik, B. T. Hjertaker, and A. Hallanger, "Gamma-ray tomography applied to hydro-carbon multi-phase sampling and slip measurements," flow measurement and instrumentation, vol. 21, no. 3, pp. 240-248, 2010.
[14] C. Sætre, G. Johansen, and S. Tjugum, "Salinity and flow regime independent multiphase flow measurements," Flow Measurement and Instrumentation, vol. 21, no. 4, pp. 454-461, 2010.
[15] R. Maad, S. Tjugum, A. Hallanger, and B. Hjertaker, "Investigation of multiphase flow blind-T mixing effectiveness using high speed gamma-ray tomometry," 09, 2016.
[16] G. A. Johansen, U. Hampel, and B. T. Hjertaker, "Flow imaging by high speed transmission tomography," Applied Radiation and Isotopes, vol. 68, no. 4-5, pp. 518-524, 2010.
[17] R. Spelay, S. Hashemi, R. Sanders, and B. Hjertaker, "Improved scatter correction model for high attenuation gamma-ray tomography measurements," Measurement Science and Technology, vol. 32, no. 8, p. 085903, 2021.
[18] G. Bal, "Inverse transport theory and applications," Inverse Problems, vol. 25, no. 5, p. 053001, 2009.
[19] S. R. Arridge and J. C. Schotland, "Optical tomography: forward and inverse problems," Inverse problems, vol. 25, no. 12, p. 123010, 2009.
[20] C. J. Elkins and M. T. Alley, "Magnetic resonance velocimetry: applications of magnetic resonance imaging in the measurement of fluid motion," Experiments in Fluids, vol. 43, no. 6, pp. 823-858, 2007.
[21] S. H. Stavland, Y. Arellano, A. Hunt, R. Maad, and B. T. Hjertaker, "Multimodal Two-Phase Flow Measurement Using Dual Plane ECT and GRT," IEEE Transactions on Instrumentation and Measurement, vol. 70, pp. 1-12, 2020.
[22] M. S. Beck, Process tomography: principles, techniques and applications. Butterworth-Heinemann, 2012.
[23] Process Tomography Ltd, "Electrical Capacitance Tomography System Type TFLR5000: Operating Manual," vol. 1. Fundamentals of ECT, ed, 2009.
[24] R. Porter, M. Fairweather, M. Pourkashanian, and R. Woolley, "The range and level of impurities in CO2 streams from different carbon capture sources," International Journal of Greenhouse Gas Control, vol. 36, pp. 161-174, 2015, https://doi.org/10.1016/.
[25] E. E. Lemmon, M. L. Huber, and M. O. McLiden. REFPROP Reference Fluid Thermodynamic and Transport Properties
[26] A. H. Harvey and E. W. Lemmon, "Method for Estimating the Dielectric Constant of Natural Gas Mixtures," International Journal of Thermophysics, vol. 26, no. 1, 2005, https://doi.org/10.1007/.
[27] I. Gordon et al., "The HITRAN2020 molecular spectroscopic database," Journal of Quantitative Spectroscopy and Radiative Transfer, vol. 277, p. 107949, 2022.
[28] A. Hunt, "Industrial Applications of High-speed Electrical Capacitance Tomography," in 9th World Congress on Industrial Process Tomography, Bath, 2019. [Online]. Available: shorturl.at/hiyzG. [Online]. Available: shorturl.at/hiyzG
[29] M. Zhang, L. Zhu, H. Wang, Y. Li, M. Soleimani, and Y. Yang, "Multiple measurement vector-based complex-valued multifrequency ECT," IEEE Transactions on Instrumentation and Measurement, vol. 70, pp. 1-10, 2020.
[30] X. Zhu, P. Dong, Q. Tu, Z. Zhu, W. Yang, and H. Wang, "Investigation of gas–solid flow characteristics in the cyclone dipleg of a pressurised circulating fluidised bed by ECT measurement and CPFD simulation," Measurement Science and Technology, vol. 30, no. 5, p. 054002, 2019.

This is the accepted version of an article published at the 2022 IEEE 12th Sensor Array and Multichannel Signal Processing Workshop (SAM)
https://doi.org/10.1109/SAM53842.2022.9827823

[31] R. Drury, "Model guided capacitance tomography: a Bayesian approach to flow regime independent multiphase flow measurement," Doctor of Philosophy, Coventry University, 2019. [Online] https://pure.coventry.ac.uk/ws/portalfiles/portal/44265288/
[32] Y. Arellano, A. Hunt, and L. Ma, "Electromagnetic technique for hydrocarbon and sand transport monitoring: proof of concept," IEEE Access, vol. 8, pp. 120766-120777, 2020.
[33] Jan Martin Kocbach et al., "Where do we stand on flow metering for CO2 handling and storage?," in International North Sea Flow Measurement Workshop, 2020, vol. 38th.
[34] E. A. Chavez Panduro et al., "Real time 3D observations of Portland Cement Carbonation at CO2 storage conditions," Environmental science & technology, vol. 54, no. 13, pp. 8323-8332, 2020.
[35] B. Brown, T. Carr, and D. Vikara, "Monitoring, verification, and accounting of CO2 stored in deep geologic formations," US Department of Energy National Energy Technology Laboratory, 2009.
[36] L. Xu, Q. Li, M. Myers, Q. Chen, and X. Li, "Application of nuclear magnetic resonance technology to carbon capture, utilisation and storage: A review," Journal of Rock Mechanics and Geotechnical Engineering, vol. 11, no. 4, pp. 892-908, 2019.
[37] S. Roussanaly, H. Deng, G. Skaugen, and T. Gundersen, "At what Pressure Shall CO2 Be Transported by Ship? An in-Depth Cost Comparison of 7 and 15 Barg Shipping," Energies, vol. 14, no. 18, p. 5635, 2021.
[38] S. Trædal, J. H. G. Stang, I. Snustad, M. V. Johansson, and D. Berstad, "CO2 Liquefaction Close to the Triple Point Pressure," Energies, vol. 14, no. 24, p. 8220, 2021.
[39] E. Pettinelli et al., "Frequency and time domain permittivity measurements on solid CO2 and solid CO2–soil mixtures as Martian soil simulants," Journal of Geophysical Research: Planets, vol. 108, no. E4, 2003.
[40] R. Sengwa, A. Soni, and B. Ram, "Dielectric behaviour of shale and calcareous sandstone of Jodhpur region," 77.22 Gm; 84.40 Xb, 2004.
[41] ATOUT. "Industry Sectors." https://atoutprocess.com/
[42] Flodatix. "Multi-dimensional flow information." https://www.flodatix.com/
[43] Ma Lu and Y. Arellano, "Apparatus For Monitoring Of The Multiphase Flow In A Pipe," GB, 182021.
[44] Industrial Tomography Systems. "ITS Products" https://www.itoms.com/

This is the accepted version of an article published at the 2022 IEEE 12th Sensor Array and Multichannel Signal Processing Workshop (SAM)
https://doi.org/10.1109/SAM53842.2022.9827823